Cellular/Molecular

Single Spine Ca^{2+} Signals Evoked by Coincident EPSPs and Backpropagating Action Potentials in Spiny Stellate Cells of Layer 4 in the Juvenile Rat Somatosensory Barrel Cortex

Thomas Nevian and Bert Sakmann
Abteilung Zellphysiologie, Max-Planck-Institut für medizinische Forschung, D-69120 Heidelberg, Germany

The precise timing of presynaptic and postsynaptic activity results in synaptic modifications, which depend on calcium influx. [Ca^{2+}] transients in the spines of spiny neurons in layer 4 (L4) of the somatosensory barrel cortex of young rats were investigated in thalamocortical brain slices by two-photon excitation microscopy to determine the spike timing dependence of the Ca^{2+} signal during near-coincident presynaptic and postsynaptic activity. [Ca^{2+}] transients evoked by backpropagating action potentials (bAPs) were mediated by voltage-dependent Ca^{2+} channels and were of comparable size in a spine and adjacent dendritic shaft. They decreased with the distance of the spine from the soma. EPSP-evoked [Ca^{2+}] transients were restricted to spine heads and were mediated almost entirely by Ca^{2+} influx through NMDA receptors (NMDARs). Their amplitude was independent of the position of the spine along the dendritic arbor. bAPs interacted with EPSPs to generate sublinear or supralinear Ca^{2+} signals in a spine when EPSP and bAP occurred within a time window of ~50 msec. Synaptic stimulation, coincident with a bAP, evoked a large postsynaptic Ca^{2+} influx that was restricted to a single spine, even after EPSPs were blocked by the AMPA receptor antagonist NBQX that rendered synapses effectively "electrically silent."

We conclude that the spines of L4 cells can act as sharply tuned detectors for patterns of APs occurring in the boutons of the afferents to L4 cells and the spines of L4 cell dendrites. The readout for near-coincident presynaptic and postsynaptic APs is a large transient Ca^{2+} influx into synaptically active spines mediated by the brief unblocking of NMDARs during the dendritic bAP.

Key words: **spine; calcium; two-photon microscopy; dendrite; coincidence detection; spiny stellate cell; barrel cortex; NMDA receptor; backpropagating action potential; EPSP**

Introduction

Ca^{2+} is an intracellular second messenger in signaling cascades of neurons, constituting a "chemical code" for their electrical activity. Ca^{2+} influx through voltage-dependent Ca^{2+} channels (VDCCs) (Westenbroek et al., 1990; Magee and Johnston, 1995) and glutamate gated ion channels (Bekkers and Stevens, 1989; Spruston et al., 1995a) located in the postsynaptic membrane of excitatory synapses result in a transient elevation of intracellular Ca^{2+} during neuronal activity (Markram and Sakmann, 1994; Spruston et al., 1995b; Helmchen et al., 1996). These Ca^{2+} channels can interact in a complex way, facilitating nonlinear Ca^{2+} signaling at a synaptic contact (Yuste and Denk, 1995; Köster and Sakmann, 1998). So far, the precise timing dependence of this nonlinear Ca^{2+} signaling is unknown.

Spiny stellate neurons in layer 4 (L4) of the barrel cortex receive whisker-specific synaptic input from cells located in the thalamic ventral posterior medial nucleus (VPM). Stellate neurons constitute the major recipient neurons for thalamocortical input and are thought to amplify and then relay excitation via their axonal arbor to other cortical layers, mostly restricted to within a barrel column (Feldmeyer et al., 1999, 2002; Lübke et al., 2000; Petersen and Sakmann, 2000, 2001; Silver et al., 2003). The dendritic arbors of stellate cells respect the barrel borders, and they are, compared with pyramidal cells, electronically and morphologically more compact. In pyramidal neurons of layer 2/3 and layer 5 of the neocortex and in pyramids of the hippocampal CA1 subfield, which have an elongated apical dendrite and a tufted dendritic arbor, the axonally initiated action potentials (APs) propagate back into the dendritic arbor and elicit a transient rise in calcium concentration ([Ca^{2+}]) (Markram et al., 1995; Yuste and Denk, 1995; Köster and Sakmann, 1998; Yuste et al., 1999). One of the functions of backpropagating APs (bAPs) in pyramidal cells is presumably to act as an induction signal for long-term changes in synaptic efficacy, depending on the coincident occurrence of presynaptic and postsynaptic APs (Markram et al., 1997a; Feldman, 2000), resulting in an highly localized transient increase in dendritic Ca^{2+} influx (Yuste and Denk, 1995; Köster and Sakmann, 1998).

Whether backpropagation of APs and the associated rise in dendritic and spinous [Ca^{2+}] is also a property of spiny stellate cells is an open question. It has been suggested that spiny stellate cells show different Ca^{2+} dynamics than cortical pyramidal cells

Received July 15, 2003; revised Dec. 4, 2003; accepted Dec. 6, 2003.

We thank H. J. Köster and V. Egger for initial help and D. J. Waters and R. M. Bruno for comments on this manuscript.

Correspondence should be addressed to Dr. Thomas Nevian, Abteilung Zellphysiologie, Max-Planck-Institut für medizinische Forschung, Jahnstrasse 29, D-69120 Heidelberg, Germany. E-mail: tnevian@mpimf-heidelberg.mpg.de.

DOI:10.1523/JNEUROSCI.3332-03.2004

 0270-6474/04/241689-11$15.00/0

(Egger et al., 1999). Synaptic connections between layer 4 spiny neurons are characterized by a relatively high NMDA receptor (NMDAR to AMPA receptor (AMPAR) ratio, which would render these connections particularly sensitive to Ca^{2+} influx during coincident bAPs and subthreshold EPSPs (Feldmeyer et al., 1999).

We have used two-photon excitation microscopy (Denk et al., 1990, 1996) to characterize the $[Ca^{2+}]$ transients in spines and dendritic shafts of spiny stellate cells. Ca^{2+} influx into spines evoked by a bAP paired with an EPSP can sum linearly, sublinearly, and supralinearly, depending strongly on the interval between bAP and EPSP and the order of occurrence.

The results suggest that in excitatory relay neurons of layer 4 of the somatosensory cortex the large $[Ca^{2+}]$ transients in single spines are part of a potential mechanism that detects the occurrence of coincident presynaptic APs in thalamic VPM or other presynaptic L4 neurons and postsynaptic APs in L4 spiny stellate neurons, respectively (Brecht and Sakmann, 2002a,b).

Materials and Methods

Slice preparation. Thalamocortical slices were prepared from the somatosensory cortex of 13- to 15-d-old (P13–P15) Wistar rats as described previously (Feldmeyer et al., 1999). All experimental procedures were in accordance with the animal welfare guidelines of the Max-Planck Society. Briefly, the rat was decapitated and the brain was quickly removed. The brain was then placed on a ramp with a 10° slope and a vertical cut at an angle of 50° was made as described by Agmon and Connors (1991). The brain was glued with the cut surface facing down onto the chilled stage of the tissue slicer. The upper part of the brain was discarded by cutting off a 3 mm thick slice. Then 350 μm thick slices were cut, incubated at 37°C for 30 min, and subsequently maintained at room temperature before recording. All experiments were performed at physiological temperatures (34–36°C).

The extracellular solution contained the following (in mM): 125 NaCl, 25 $NaHCO_3$, 2.5 KCl, 1.25 NaH_2PO_4, 1 $MgCl_2$, 25 glucose, and 2 $CaCl_2$, bubbled with 95% O_2 and 5% CO_2. A 10 μM concentration of glycine was always added to the extracellular solution (Johnson and Ascher, 1987).

Electrophysiology. Patch pipettes (5–7 MΩ) for whole-cell voltage recording were filled with a solution containing the following (in mM): 125 K-gluconate, 20 KCl, 10 HEPES, 4 ATP-Mg, 10 Na-phosphocreatine, and 0.3 GTP and a Ca^{2+} indicator, Oregon Green 488 BAPTA-1 (OGB1; 200 μM; Molecular Probes, Eugene, OR). The barrel field of the rat somatosensory cortex and individual spiny neurons were visualized using infrared (IR) gradient contrast videomicroscopy (Dodt and Zieglgänsberger, 1998). The barrels appeared in layer 4 as evenly spaced dark structures, separated by lighter septa (Feldmeyer et al., 1999; Lübke et al., 2000; Petersen and Sakmann, 2000). The somata of spiny neurons in layer 4 tended to cluster at the barrel borders and were identified by their shape and size (10–15 μm in diameter) and by the star-like initial parts of their dendrites lacking a prominent apical dendrite. Recordings were made from cells located between 50 and 100 μm below the slice surface (Stuart et al., 1993) in the whole-cell (wc) recording configuration with a patch-clamp amplifier (EPC-9/2; List-Electronics, Darmstadt, Germany) operated in current-clamp or voltage-clamp mode. The voltage signals were filtered at 3 kHz and digitized at 10 kHz by the integrated analog-to-digital converter. Initial access resistance was <15 MΩ. Cells were filled for at least 20 min with OGB1 before fluorescence measurements to allow equilibration of the indicator concentration between the patch pipette and the cytoplasm.

Pharmacological compounds. Na^+ channels were blocked by tetrodotoxin (TTX; 1 μM), VDCCs by Cd^{2+} (100 μM), AMPA receptors by 1,2,3,4-tetrahydro-6-nitro-2,3-dioxo-benzoquinoxaline-7-sulfonamide (NBQX; 10 μM), NMDA receptors by D-5-amino-phosphonopentanoic acid (APV; 25 μM) and group II metabotropic glutamate receptors by 2-(*S*)-α-ethylglutamic acid (EGlu; 50 μM). All compounds were purchased from Tocris (Bristol, UK).

Calcium imaging. A galvanometer scanning unit (TCSNT; Leica Microsystems, Mannheim, Germany) was attached to an upright microscope (DMLFS; Leica) equipped with a 63× objective (HCX APO W63x UVI; numerical aperture, 0.9; Leica). For two-photon excitation, short pulses of 170–200 fsec at 76 MHz from a Ti:Sa-Laser (MIRA 900F; Coherent, Santa Clara, CA) at 870–890 nm pumped by a solid-state laser (Verdi 5W; Coherent) were used. Line-scan imaging was performed with high temporal resolution (2.2 msec/line). External non-descanned detection behind the objective and the condenser was used, yielding a high signal-collection efficiency. Transmission and epifluorescence signals were recorded by photomultiplier tubes (R6357; Hamamatsu Photonics, Herrsching, Germany) and summed offline (Köster et al., 1999). Line-scan imaging and electrical recordings were synchronized by a hardware trigger supplied by the scanner electronics.

The distance from the soma was extrapolated from small linear segments placed online along the dendritic branches. This tracing method underestimated the exact distance, derived from a reconstruction of the dendritic length from a three-dimensional fluorescence stack, by <10% ($n = 4$).

Simultaneously with full-frame fluorescence image acquisition, IR-scanning gradient contrast (IR-SGC) images were recorded (Rathenberg et al., 2003). The transmitted IR laser light was imaged through a gradient-contrast tube (Dodt et al., 1999) onto a photomultiplier.

Data analysis. Fluorescence line-scan images were analyzed using custom software macros based on the Leica confocal software. A line was scanned every 2.2 msec, and two lines were averaged offline, resulting in a temporal resolution of 4.4 msec. The fluorescence for each time point was averaged for regions of interest (ROIs) enclosing the dendrite or spine examined. Before stimulation, fluorescence was averaged for 100 msec to obtain the basal fluorescence F_0. A region distant to any indicator-containing structure was chosen to determine the background fluorescence F_B. Background fluorescence was independent of the size and position of the background ROI, indicating a homogeneous background along the scan line. Relative fluorescence changes were calculated as $\Delta F/F(t) = (F(t) - F_0)/(F_0 - F_B)$. Assuming a constant background, $\Delta F/F$ is slightly underestimated but independent of the size of the neuronal compartment (Sabatini et al., 2002). Single exponential fits to the decay of the fluorescence transients yielded the peak amplitude, denoted as A, and the decay time constant τ. Fluorescence traces are averages of two to five trials. Data are represented as means ± SD. Differences between groups were evaluated using Student's *t* test (either paired or two-tailed unpaired) and statistical significance was asserted for $p < 0.05$. The number of spines, each of which was measured in a different cell, is given by *n*.

Dye saturation. Peak $[Ca^{2+}]$ transient amplitudes might be underestimated when the high-affinity Ca^{2+} indicator OGB1 is used because of saturation. The linearity of the fluorescence increase, as reported by the dye, was evaluated from $[Ca^{2+}]$ transients evoked by two bAPs separated by different time intervals Δt ($n = 8$). These sequences resulted in $[Ca^{2+}]$ transients with two peaks corresponding to each bAP. The peak amplitude, A_{2APs}, was derived from a single exponential fit to the decay of the $[Ca^{2+}]$ transient. A_{2APs} increased with shorter time intervals (supplementary Fig. 1*A*) to 0.95 ± 0.28 at $\Delta t = 10$ msec. This value was much smaller than the maximal increase in fluorescence (2.55 ± 0.52) evoked by a train of 20 APs at 100 Hz.

Normalizing A_{2APs}, derived from the AP–AP sequence, to the linear sum of a $[Ca^{2+}]$ transient evoked by a single bAP ($A_{AP} = 0.46 \pm 0.16$ and $\tau_{AP} = 490 \pm 190$ msec) gave a measure for the linearity of the dye (denoted as the "nonlinearity factor"). The nonlinearity factor was close to unity for all time intervals tested between 10 and 300 msec, indicating linear summation of the $[Ca^{2+}]$ transients evoked by two bAPs (supplementary Fig. 1*B*). Comparing A_{2APs} to the predicted linear sum for each measurement showed no significant difference (paired *t* test; $p > 0.1$; $n = 6$). Thus, at least up to $A_{2APs} = 1$, the nonlinearity factor faithfully reported the linear summation of two AP-evoked $[Ca^{2+}]$ transients.

Results

Identification of active synaptic contacts in spiny neurons

Spiny stellate neurons in layer 4 of the barrel cortex were loaded with the Ca^{2+} indicator Oregon Green 488 BAPTA-1 via the

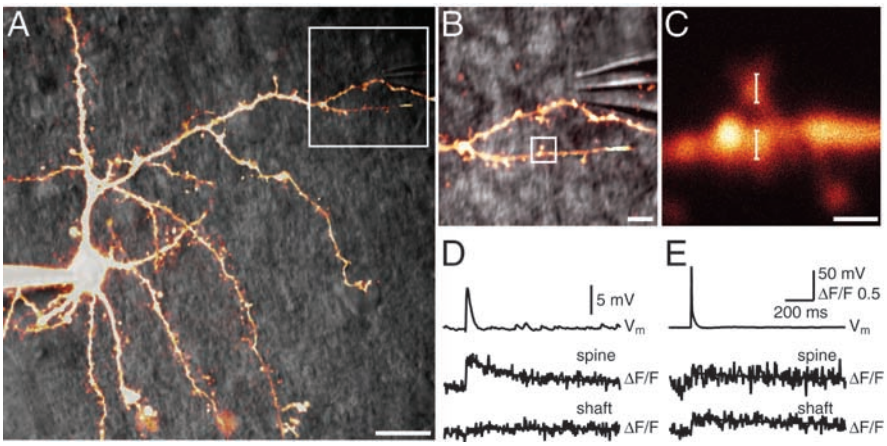

Figure 1. Two-photon imaging of spiny neurons. *A*, Maximum projection of a fluorescence stack (25 images; axial step size, 2 μm) of a spiny neuron overlaid with the IR-SGC image of one optical section visualizing the surrounding tissue and the stimulation electrode (top right). *B*, Magnified view of the boxed region in *A*. The stimulation electrode was placed in the vicinity of a dendrite and then an active contact was located. The active spine in this case is included in the box. *C*, Higher-magnification image of the active spine in *B*. The position of the line scan through the spine and shaft and the regions of interest in which fluorescence was averaged are indicated by the vertical lines. Scale bars: *A*, 20 μm; *B*, 5 μm; *C*, 1 μm. *D*, Somatic whole-cell recording of an EPSP (top trace), the corresponding $[Ca^{2+}]$ transient recorded in the active spine (middle trace), and the adjacent dendritic shaft (bottom trace) shown in *C*. The resting membrane potential was −71 mV. A clear rise in fluorescence was observed in the spine head ($A_{EPSP} = 0.50 \pm 0.15$), but no increase in fluorescence was seen in the shaft ($A_{EPSP} = 0.09 \pm 0.08$). *E*, Fluorescence $[Ca^{2+}]$ transients in the same spine (middle trace) and shaft (bottom trace) evoked by a bAP (top trace). The bAP gave rise to a similar fluorescence transient in the spine head ($A_{AP} = 0.24 \pm 0.01$) and in the dendritic shaft ($A_{AP} = 0.23 \pm 0.01$).

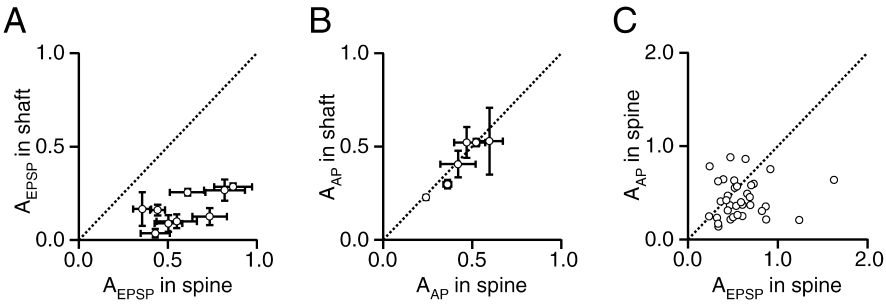

Figure 2. $[Ca^{2+}]$ transients in spines and shafts of spiny neurons. *A*, Peak $[Ca^{2+}]$ transient amplitude elicited by an EPSP (A_{EPSP}) measured in the shaft versus peak amplitude in the spine. All points fall below the unity line (dashed line), indicating that the $[Ca^{2+}]$ transient in the shaft was much smaller than in the spine head (reduction to 26 ± 12%; $p < 0.0001$; $n = 9$). *B*, bAP-evoked $[Ca^{2+}]$ transients measured in spines and shafts showed a similar peak fluorescence amplitude A_{AP} (105 ± 10%; $p > 0.3$; $n = 6$). *C*, Plot of the mean peak $[Ca^{2+}]$ transient amplitude evoked by a bAP versus the mean peak $[Ca^{2+}]$ transient amplitude evoked by an EPSP in the same spine. A total of 24 of 35 points fall below the unity line (dashed line), indicating a larger Ca^{2+} influx evoked by synaptic stimulation. Each data point in *A–C* represents a spine of a different cell.

patch pipette in the wc recording configuration. After filling, their morphology became visible in the two-photon excitation (TPE) fluorescence image (Fig. 1*A*). The tip of an extracellular stimulation pipette was positioned in close proximity to a dendritic branch (~5 μm) under visual control (Fig. 1*B*) using the overlay of the IR-scanning gradient contrast (IR-SGC) image with the TPE fluorescence image of the indicator loaded cell.

Active synaptic contacts were identified in the full-frame, continuous image acquisition mode (500 msec/frame) by a localized, transient increase in fluorescence after synaptic stimulation. Spines responding with a $[Ca^{2+}]$ transient (Fig. 1*C,D*) were located at distances ranging between 30 and 210 μm from the soma (79 ± 35 μm; $n = 46$). Putative shaft synapses were found only infrequently ($n = 2$), and $[Ca^{2+}]$ transients in these contacts were not different from spine synapses.

The stimulation strength was set to evoke reliable EPSPs, with peak amplitudes between 1 and 11 mV (6 ± 3 mV; $n = 29$). This reflected the activation of, on average, four connections with a total of ~12 synaptic contacts during an EPSP [assuming a mean EPSP amplitude of 1.6 mV and three synaptic contacts per layer 4 connection (Feldmeyer and Sakmann, 2000)]. In the vicinity of an active spine (~20 μm) no other spines were observed that responded, suggesting that the other synaptic contacts contributing to the EPSP were located far from the particular spine under investigation. Once an active spine was found, almost every stimulus evoked a transient rise in $[Ca^{2+}]$. The failure rate was <10% ($n = 10$ spines), which is in agreement with results reported for connected pairs of spiny stellate cells (Feldmeyer et al., 1999).

$[Ca^{2+}]$ transients in spines and shafts

Figure 1*D* shows an EPSP (top trace) and the simultaneously recorded $[Ca^{2+}]$ transient evoked by synaptic stimulation in the spine and shaft shown in Figure 1*C*. The Ca^{2+} signal was almost completely restricted to the spine head. In a plot of the peak $[Ca^{2+}]$ transient amplitudes (A_{EPSP}) in shafts versus peak amplitudes in spine heads, all data points fell clearly below unity (Fig. 2*A*). The peak amplitude of the small signal in the shaft was correlated with the peak amplitude in the spine (linear regression; $r = 0.75$). On average, the peak amplitude in the shaft was 26 ± 12% of the peak amplitude in the spine head ($n = 9$; paired t test; $p < 0.0001$).

The $[Ca^{2+}]$ transients evoked by bAPs were measured in the same spines and shafts ($n = 6$). In Figure 1*E*, the bAP-evoked peak $[Ca^{2+}]$ transient amplitudes (A_{AP}) were similar in the shaft and spine. The peak amplitudes in shafts plotted versus the peak amplitudes in spine heads fell almost exactly on the unity line (Fig. 2*B*). The mean ratio of the peak amplitude in the shaft compared with that in the spine was 105 ± 10% (paired t test; $p > 0.2$). The bAP-evoked $[Ca^{2+}]$ transient was almost completely blocked (7 ± 5% of control; $n = 4$) after bath application of Cd^{2+} (100 μM), indicating Ca^{2+} influx through VDCCs. The bAP-evoked $[Ca^{2+}]$ transients represent a global dendritic signal common to spines and shafts, whereas EPSP-evoked $[Ca^{2+}]$ transients are spatially confined to the spine head. The small shaft Ca^{2+} signal recorded after synaptic stimulation was presumably caused by the diffusion of Ca^{2+} between the spine and the shaft (Svoboda et al., 1996), although most of the Ca^{2+} in a spine was cleared by other mechanisms, such as Ca^{2+} pumps.

The peak $[Ca^{2+}]$ transient evoked by an EPSP in a spine head was larger than the corresponding transient evoked by a bAP (Fig. 2*C*) in 70% (24 of 35) of the spines. The mean peak amplitude evoked by an EPSP was $A_{EPSP} = 0.58 \pm 0.27$ ($n = 47$), compared with $A_{AP} = 0.44 \pm 0.20$ in the case of a bAP-evoked $[Ca^{2+}]$ transient ($n = 36$), which was significantly larger (paired t test;

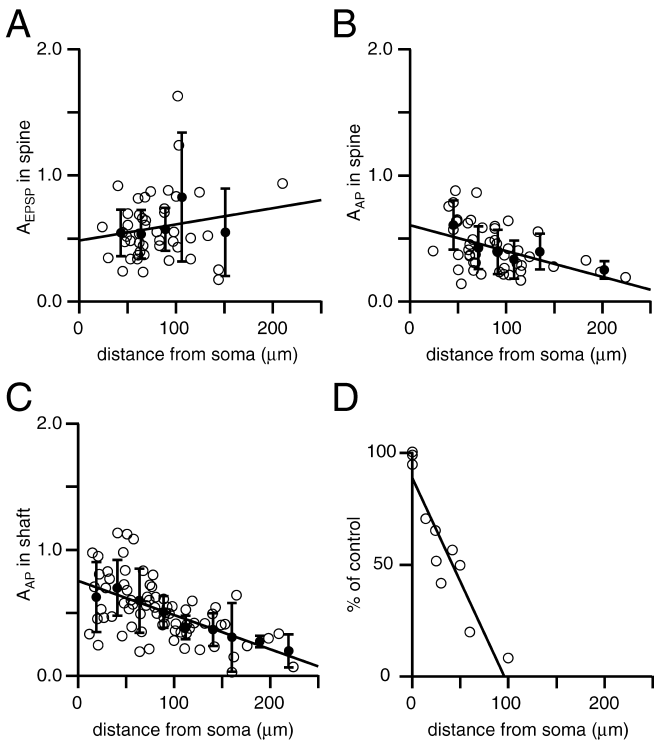

Figure 3. Distance dependence of the peak $[Ca^{2+}]$ transient amplitude in a spine evoked by bAPs and EPSPs. *A*, Peak $[Ca^{2+}]$ transient amplitude (A_{EPSP}) evoked by an EPSP as a function of the distance of the spine from the soma. Open circles represent individual spines ($n = 47$). Filled circles represent mean amplitudes binned for 25 μm intervals of dendritic lengths up to 125 μm from the soma and the mean amplitude for spines >125 μm from the soma. The solid line is a linear regression ($r = 0.16$). *B*, A_{AP} evoked by a bAP in spines as a function of the distance of the spine from the soma. Open circles represent individual spines ($n = 36$). Filled circles represent mean amplitudes binned for 25 μm intervals of dendritic lengths up to 150 μm from the soma and the mean amplitude for spines >150 μm from the soma. The solid line is a linear regression ($r = -0.44$). *C*, A_{AP} evoked by a bAP in the dendritic shaft as a function of the distance from the soma (9 cells). Open circles represent individual measurements. Filled circles represent mean amplitudes binned for 25 μm intervals of dendritic length. The solid line is a linear regression ($r = -0.55$). *D*, Attenuation of dendritic $[Ca^{2+}]$ transients after bath application of TTX (1 μM) with the distance from the soma. AP waveforms were used as voltage commands in voltage clamp, and they were scaled to elicit $[Ca^{2+}]$ transients close to the soma of similar size to control conditions (100% of control; 3 cells). The solid line represents a linear regression ($r = -0.93$).

$p < 0.01$). The decay time constants were not significantly different for EPSP-evoked ($\tau_{EPSP} = 384 \pm 203$ msec) and bAP-evoked ($\tau_{AP} = 432 \pm 209$ msec) $[Ca^{2+}]$ transients (paired *t* test; $p > 0.4$).

Dependence of $[Ca^{2+}]$ transients in spines on the distance from the soma

The relative size of $[Ca^{2+}]$ transients evoked by either an EPSP or a bAP showed different dependencies on the distance of the spine from the soma. The EPSP-evoked peak $[Ca^{2+}]$ transient was independent of the distance from the soma (Fig. 3*A*) ($r = 0.16$; $n = 47$). In contrast, the peak $[Ca^{2+}]$ transient amplitude evoked by a bAP in spines decreased with the distance from the soma (Fig. 3*B*) (linear regression; $r = -0.44$; $n = 49$), in agreement with the distance dependence measured for bAP-evoked $[Ca^{2+}]$ transients in dendritic shafts (Fig. 3*C*) ($r = -0.55$). Comparing the mean A_{AP} values close to the soma (distance <50 μm) to those in the distal segments (distance >150 μm) showed a reduction in the bAP-evoked $[Ca^{2+}]$ transients to 41% of the soma value (unpaired *t* test; $p < 0.005$).

To test whether the $[Ca^{2+}]$ transients were evoked by actively backpropagating APs, the spread of the $[Ca^{2+}]$ transient within the dendritic arbor was measured in voltage clamp for control and after bath application of TTX (1 μM). Somatic AP waveforms, recorded in current clamp, were used as voltage commands in voltage clamp (Stuart and Sakmann, 1994). In this recording configuration, $[Ca^{2+}]$ transients were acquired along the dendritic arbor as controls. Bath application of TTX abolished the $[Ca^{2+}]$ transients. Waveforms were scaled by a factor of 1.5–2 to elicit $[Ca^{2+}]$ transients close to the soma with the same amplitude as in the control measurements (Kaiser et al., 2001). This procedure ensured that the applied AP waveform activated VDCCs in the same way as under control conditions. $[Ca^{2+}]$ transients in the presence of TTX were strongly attenuated compared with control (Fig. 3*D*).

The decay time constants of EPSP-evoked ($r = 0.08$) and AP-evoked ($r = 0.08$) $[Ca^{2+}]$ transients in spines were independent of the distance of the spine from the soma (data not shown).

These results indicate that dendritic $[Ca^{2+}]$ transients are evoked by actively backpropagating APs.

$[Ca^{2+}]$ transients evoked by pairing EPSP and bAP depend on the interstimulus interval

To examine the interaction of synaptic potentials with bAPs, EPSPs and bAPs were paired at different time intervals. This pairing resulted in very different $[Ca^{2+}]$ transients with linear, sublinear, and supralinear summation of the Ca^{2+} signals, depending on the interval between the two stimuli and on their order of occurrence (Fig. 4).

EPSP- and bAP-evoked $[Ca^{2+}]$ transients in a spine were recorded individually as controls, and exponential fits to the decay of the $[Ca^{2+}]$ transients yielded the peak $[Ca^{2+}]$ amplitudes A_{EPSP} and A_{AP} and the corresponding decay time constants τ_{EPSP} and τ_{AP}, respectively (Fig. 4*B*). Then EPSP and bAP were paired at an interstimulus interval Δt (measured between the onset of the extracellular stimulus and the peak of the AP), resulting in $[Ca^{2+}]$ transients with two peaks. A single exponential fit to the decay time course of the $[Ca^{2+}]$ transient, evoked by the paired stimuli, yielded the peak amplitude A_{paired} and the decay time constant τ. A_{paired} normalized to the linear sum of the control stimuli for the corresponding time interval is referred to as the nonlinearity factor. A value of 1 corresponds to linear summation of both Ca^{2+} signals.

Supralinear summation was found when the EPSP preceded the bAP by 10 msec (Fig. 4*D*). The peak $[Ca^{2+}]$ transient amplitude for this pairing sequence was, on average, 1.7 ± 0.2-fold larger than the expected linear sum ($n = 13$). In contrast, when the EPSP followed the AP with a delay of 50 msec, the $[Ca^{2+}]$ transients summed sublinearly (i.e., the peak $[Ca^{2+}]$ transient amplitude was smaller than the expected linear sum) in all spines tested (Fig. 4*C*). The nonlinearity factor for the AP–EPSP pairing sequence was, on average, 0.86 ± 0.08 ($n = 7$).

Peak $[Ca^{2+}]$ transient amplitude dependence on interval between EPSP and bAP

The interval between bAP and EPSP was varied between −300 and 300 msec and yielded a plot for the spike-timing dependence of the peak $[Ca^{2+}]$ amplitude. Negative time intervals ($\Delta t < 0$) denote the pairing sequence AP–EPSP, positive intervals ($\Delta t > 0$) denote the pairing sequence EPSP–AP. Figure 5*A* shows averages of peak $[Ca^{2+}]$ amplitudes A_{paired} plotted versus the time interval Δt between the two stimuli. Comparing A_{paired} for adjacent time points revealed a significant increase in the $[Ca^{2+}]$ transient from $\Delta t = 1$ to $\Delta t = 10$ msec (unpaired *t* test; $p < 0.005$) and a

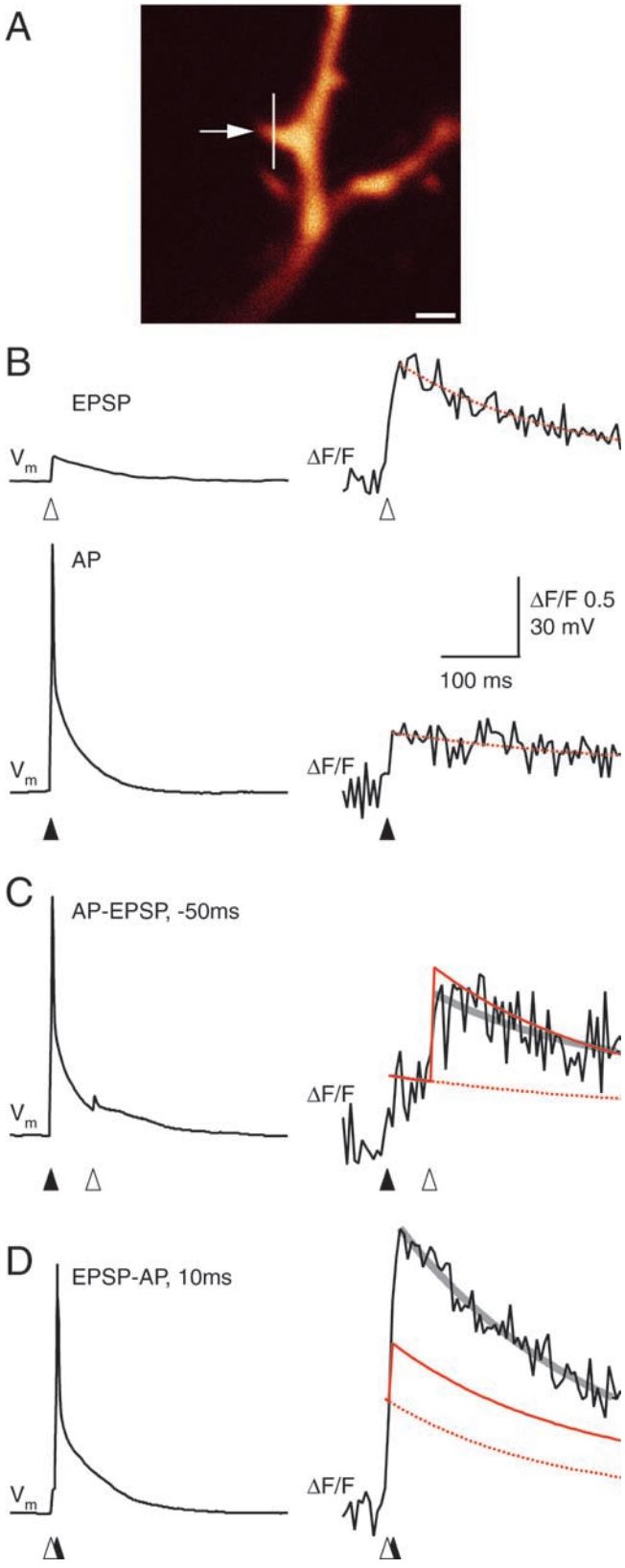

Figure 4. Pairing of bAPs and EPSPs evokes nonlinear Ca^{2+} influx. *A*, Fluorescence image of a dendritic region with an active synaptic contact (white arrow). The white line indicates the position of the line scan. Scale bar, 2 μm. *B*, Somatic voltage recordings (left) and the corresponding [Ca^{2+}] transients (right) for EPSP (top trace) and bAP (bottom trace), respectively. The resting membrane potential was −71 mV. The red dashed lines represent single exponential fits to the single-stimulus evoked control transients yielding $A_{EPSP} = 0.70$ and $A_{AP} = 0.37$. Open and filled arrowheads indicate the onset of the EPSP and AP, respectively. *C*, Pairing of a bAP preceding an EPSP by 50 msec (somatic voltage recording, left). The resulting [Ca^{2+}] transient is shown to the right. The red dashed line indicates the bAP-evoked [Ca^{2+}] transient, and the solid red line is the predicted linear sum of the control stimuli derived from *B*, indicating sublinear summation of the [Ca^{2+}] transients. The solid gray line represents the single exponential fit to the decay of the [Ca^{2+}] transient, yielding the peak amplitude A_{paired}. In this case $A_{paired} = 0.86$ is smaller than the predicted linear sum of 1.02, resulting in a nonlinearity factor of 0.84. *D*, Pairing of an EPSP with a following bAP at a stimulus interval of 10 msec (somatic voltage recording, left) and the corresponding [Ca^{2+}] transient (right). The red dashed line indicates the EPSP-evoked [Ca^{2+}] transient, and the solid red line is the predicted linear sum of the control stimuli derived from *B*, indicating a supralinear summation of the [Ca^{2+}] transients. The solid gray line is the single exponentials fit to the decay of the [Ca^{2+}] transient, yielding the peak amplitude $A_{paired} = 1.78$. The linear sum in this case is 1.03, resulting in a nonlinearity factor of 1.72.

significant decrease from $\Delta t = 50$ to $\Delta t = 100$ msec ($p < 0.05$). The average peak [Ca^{2+}] amplitude in this interval was A_{paired} (10 msec $\leq \Delta t \leq$ 50 msec) = 1.52 ± 0.46. For all other intervals the amplitudes were not significantly different. Comparing A_{paired} for any pair of time points for $\Delta t <$10 msec and $\Delta t >$50 msec also did not indicate significant differences ($p > 0.05$). Pooling the peak amplitudes in these intervals yielded A_{paired} = 0.91 ± 0.30. Thus, only when an EPSP is followed by a bAP within 10–50 msec is a significantly increased Ca^{2+} influx generated (unpaired *t* test; $p < 10^{-6}$).

The decay of the [Ca^{2+}] transients evoked by paired stimuli did not depend on the stimulus interval, or on the order of occurance of EPSP and AP. The average decay time constant for the paired stimuli was $\tau = 375 \pm 119$ msec, similar to the decay times of the single stimulus-evoked transients ($p > 0.2$).

Nonlinear summation of Ca^{2+} signals

The increased peak [Ca^{2+}] transient amplitudes for the sequence EPSP–AP between 10 and 50 msec was the result of nonlinear summation of Ca^{2+} signals. Figure 5*B* shows the nonlinearity factor as a function of the interstimulus interval. It reveals the time domains of linear, sublinear, and supralinear summation. Comparing the peak amplitude A_{paired} to the predicted linear sum for each time interval yielded a significant supralinear summation for the time intervals $\Delta t = 10$ msec ($p < 0.0001$; $n = 13$), 20 msec [nonlinearity factor (20 msec) = 1.5 ± 0.3; $p < 0.0001$; $n = 13$], and 50 msec [nonlinearity factor (50 msec) = 1.3 ± 0.1; $p < 0.005$; $n = 5$]. A significant sublinear summation was found for $\Delta t = -50$ msec (paired *t* test; $p < 0.005$; $n = 7$). For all other interstimulus intervals, deviations from the linear sum were insignificant ($p > 0.2$).

Thus, supralinear summation of Ca^{2+} signals in single spines evoked during pairing of EPSPs and bAPs was restricted to a relatively short time window of 50 msec and to the sequence EPSP–AP. This time window can, for spiny stellate cell synapses, be denoted as a "coincidence time window," during which the occurrence of presynaptic and postsynaptic APs is encoded by an increased Ca^{2+} influx as opposed to the uncorrelated occurrence of presynaptic and postsynaptic APs outside of this time window. Reversing the order of stimulation (AP–EPSP) resulted either in linear summation of Ca^{2+} signals or in sublinear summation for $\Delta t = -50$ msec.

Time course of supralinear summation

The Ca^{2+} influx evoked by a bAP, if preceded by an EPSP in the coincidence time window, was larger than the Ca^{2+} influx evoked by a bAP alone. Normalizing the rise in [Ca^{2+}] evoked by the bAP (A'_{AP}) in the sequence EPSP–AP to the rise in [Ca^{2+}] by

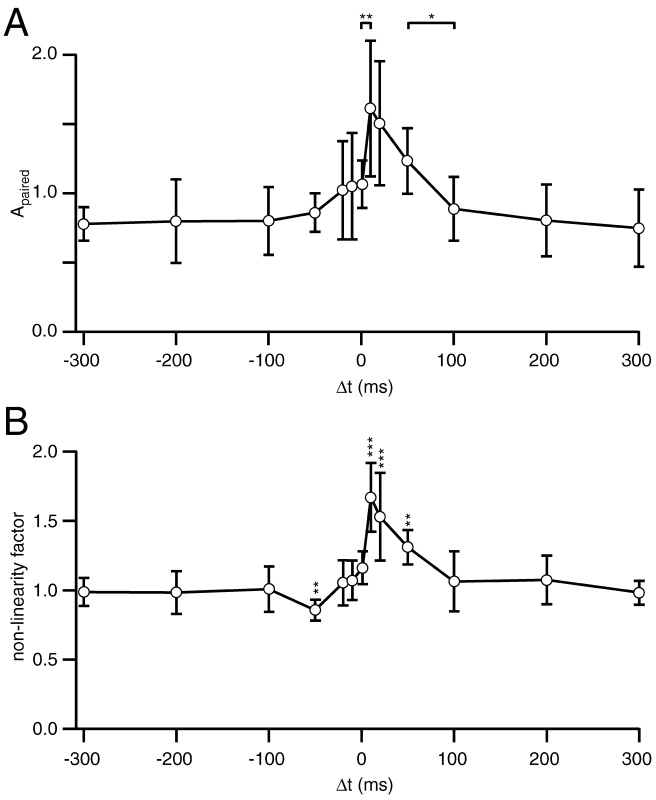

Figure 5. Peak $[Ca^{2+}]$ transient amplitudes and nonlinear Ca^{2+} signaling evoked by pairing EPSPs with bAPs at different time intervals. *A*, The peak $[Ca^{2+}]$ transient amplitudes evoked by pairing EPSPs with bAPs, A_{paired}, are plotted for the corresponding time intervals Δt. Negative times denote the sequence AP–EPSP and positive times denote the sequence EPSP–AP. Significant differences between the peak amplitudes of neighboring time points were found between $\Delta t = 1$ and $\Delta t = 10$ msec (**$p < 0.005$; Student's *t* test) and between $\Delta t = 50$ and $\Delta t = 100$ msec (*$p < 0.05$). *B*, The nonlinearity factor at different interstimulus intervals. The nonlinearity factor was defined as the ratio of the peak $[Ca^{2+}]$ transient amplitude, A_{paired}, to the corresponding linear sum. Significant differences between the peak amplitudes and the linear sum were found for $\Delta t = -50$ msec (**$p < 0.005$; paired *t* test; $n = 7$) where the $[Ca^{2+}]$ transients added sublinearly, $\Delta t = 10$ msec (***$p < 0.0001$; $n = 13$), $\Delta t = 20$ msec (***$p < 0.0001$; $n = 13$), and $\Delta t = 50$ msec (**$p < 0.005$; $n = 5$). In the latter cases, the amplitudes A_{paired} were larger than the linear sum. The maximum was found at $\Delta t = 10$ msec, at which the EPSP–AP evoked $[Ca^{2+}]$ transient was 1.7-fold larger than expected.

a control bAP (A_{AP}) is a measure for the EPSP-timing-dependent potentiation of the bAP-evoked $[Ca^{2+}]$ transient ("EPSP–AP potentiation"). The potentiation (A'_{AP}/A_{AP}) was 2.3 ± 0.5, 2.1 ± 0.7, and 1.4 ± 0.3 for $\Delta t = 10$, 20, and 50 msec, respectively (Fig. 6*A*).

The EPSP–AP potentiation (with a maximum at $\Delta t = 10$ msec) decayed along an exponential time course, with a time constant of 32 msec (Fig. 6*A*). This value matches the decay time constant of the NMDAR-mediated component of EPSCs in spiny stellate cells [$\tau_{NMDAR} = 35 \pm 15$ msec (Feldmeyer et al., 1999)] and suggests that the mechanism generating the supralinear Ca^{2+} influx during near-coincident presynaptic and postsynaptic APs is determined mostly by the closing kinetics of synaptic NMDAR channels. A bAP following an EPSP relieves the Mg^{2+} block of the synaptic NMDAR channels, which are in an open state after the binding of glutamate, but still remain Ca^{2+}-impermeable because of the voltage-dependent Mg^{2+} block. With an increasing interstimulus interval between EPSP and bAP, fewer NMDARs are in an open (but blocked) state, and the effect of the membrane depolarization during the bAP is correspondingly smaller.

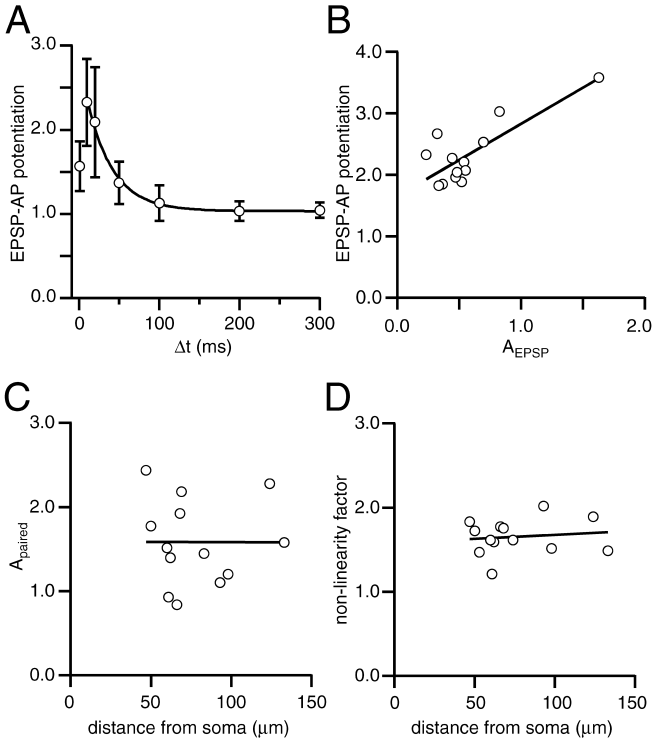

Figure 6. The nonlinearity corresponds to the NMDAR channel kinetics and is independent of spine location. *A*, EPSP–AP potentiation as a function of the stimulus interval Δt. The solid line represents a single exponential fit to the points for $\Delta t \geq 10$ msec. The fit yielded a decay time constant of the EPSP–AP potentiation of 32 msec. This value corresponded well to the reported decay of the NMDAR component of EPSCs measured in spiny neurons ($\tau_{NMDA} = 35$ msec). *B*, The EPSP–AP potentiation for $\Delta t = 10$ msec scaled with the EPSP-evoked peak $[Ca^{2+}]$ amplitude A_{EPSP}, indicating a common source of the Ca^{2+} influx. The solid line represents a linear fit ($r = 0.8$; $n = 13$). *C*, Plot of the peak $[Ca^{2+}]$ transient amplitude, A_{paired}, for the sequence EPSP–AP at $\Delta t = 10$ msec versus the distance of the spine from the soma. The linear regression line showed no correlation ($r = -0.002$; $n = 13$). *D*, The nonlinearity factor for the sequence EPSP–AP at $\Delta t = 10$ msec is independent of the distance of a spine from the soma (solid line; linear regression; $r = 0.12$; $n = 13$).

Additional evidence that the bAP-evoked supralinear $[Ca^{2+}]$ transient is "probing" the number of open NMDARs was the value of the EPSP–AP potentiation at $\Delta t = 1$ msec. At this interval (assuming fast propagation of the AP into the dendritic arbor within <1 msec) the number of open NMDARs was not yet maximal because of the slow opening kinetics of NMDARs [reflected in the rise time of 5–10 msec of the NMDAR-mediated EPSC (Feldmeyer et al., 1999)]. The potentiation was smaller at $\Delta t = 1$ than at $\Delta t = 10$ msec, when more NMDARs were open.

The EPSP–AP potentiation for the sequence EPSP–AP at $\Delta t = 10$ msec scaled with the size of the EPSP-evoked peak $[Ca^{2+}]$ transient amplitude ($r = 0.8$; $n = 13$) (Fig. 6*B*). Again, this is consistent with the view that the main source of the supralinear Ca^{2+} influx is synaptic NMDAR channels.

Dependence of spine $[Ca^{2+}]$ transients evoked by coincident activity on distance from soma

The decrease of the peak $[Ca^{2+}]$ amplitude evoked by a bAP with the distance from the soma suggested that coincidence effects in spines might be sensitive not only to the order and interval between EPSP and bAP but might depend, in addition, on the location of a spine. A_{paired} of $[Ca^{2+}]$ transients evoked by the sequence EPSP–AP at $\Delta t = 10$ msec plotted against the distance of a spine from the soma showed no correlation ($r = -0.002$) (Fig.

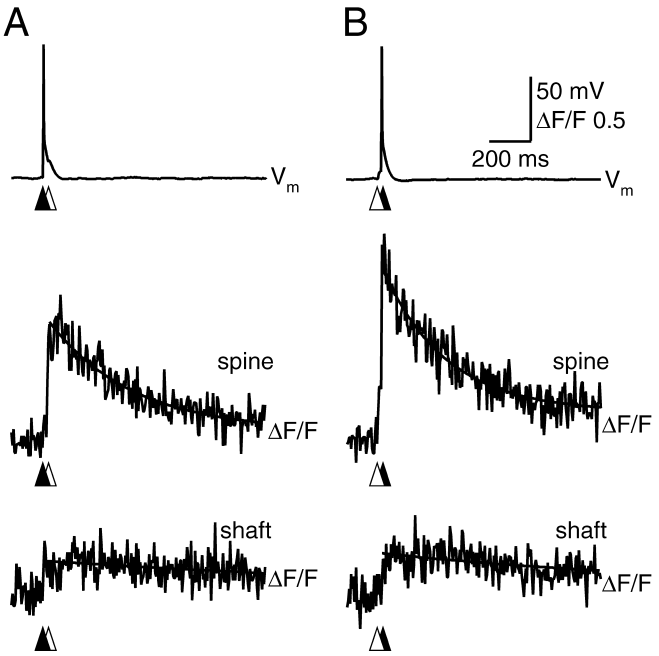

Figure 7. Supralinear $[Ca^{2+}]$ transients are restricted to the spine head. *A*, The top trace shows the somatic voltage recording of an EPSP 20 msec after an AP. The sequence AP–EPSP resulted in a larger $[Ca^{2+}]$ transient in the spine head (middle trace) compared with the adjacent shaft (bottom traces). The recording is from the spine shown in Figure 1. *B*, The top trace shows the somatic voltage recording of an EPSP preceding an AP by 20 msec. The corresponding $[Ca^{2+}]$ transients in the active spine (middle trace) and adjacent shaft illustrate that the large supralinear $[Ca^{2+}]$ transient in this case was restricted exclusively to the spine head ($A_{paired} = 1.35 \pm 0.02$ in the spine head compared with $A_{paired} = 0.36 \pm 0.07$ in the shaft). The fluorescence increase in the shaft was caused by Ca^{2+} influx evoked by the bAP. Note that the peak amplitude in the spine for the sequence AP–EPSP is smaller than for the sequence EPSP–AP during the same interval.

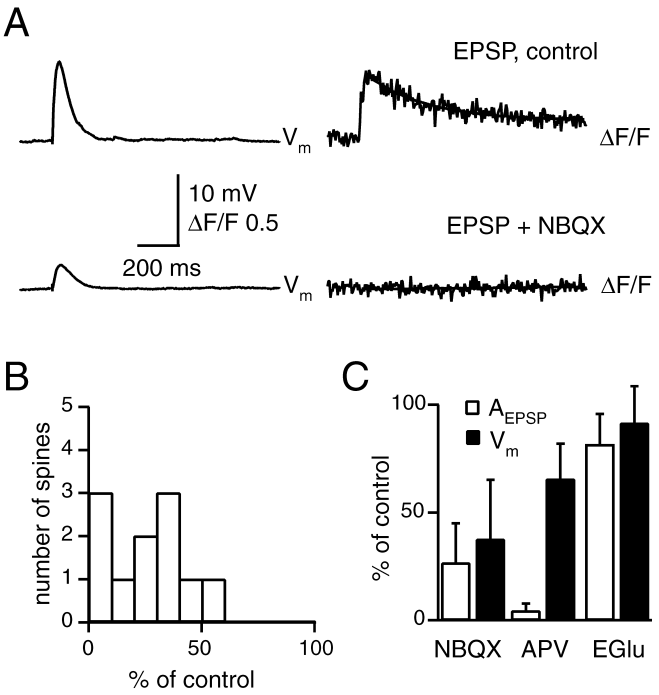

Figure 8. Influence of glutamate receptors on synaptic EPSP-evoked $[Ca^{2+}]$ transients. *A*, Somatic voltage recordings (left) and $[Ca^{2+}]$ transients (right) in an active synaptic contact evoked by an EPSP for control conditions (top traces) and after bath application of the AMPA-receptor channel-blocker NBQX (10 μM, bottom traces). Note the complete block of the spinous $[Ca^{2+}]$ transient in this case. The resting membrane potential was −70 mV. *B*, Histogram of the reduction of $[Ca^{2+}]$ transient amplitudes by NBQX ($n = 11$). The reduction varied greatly. In three spines the $[Ca^{2+}]$ transient amplitude was blocked almost completely. *C*, Average reduction of the peak $[Ca^{2+}]$ transient amplitude (white columns) and the somatically recorded EPSP amplitude (black columns) after bath application of glutamate-channel blockers. The EPSP amplitude after the application of NBQX was reduced to 38 ± 28% of control. The $[Ca^{2+}]$ transient amplitude was reduced to 27 ± 18% of control in this case. Application of APV blocked the $[Ca^{2+}]$ transient amplitude to 4 ± 3% of control, and the EPSP amplitude was reduced to 66 ± 17% of control. The mGluR blocker EGlu did not reduce the EPSP-evoked $[Ca^{2+}]$ transient amplitude (82 ± 14% of control) or the somatic EPSP amplitude (92 ± 18% of control).

6*C*). The nonlinearity factor was also independent of the distance of a spine from the soma ($r = 0.1$) (Fig. 6*D*).

Thus, the size of the Ca^{2+} influx and the nonlinearity factor during near-coincident presynaptic and postsynaptic APs were independent of the position of the synaptic contact along the dendritic arbor. The membrane depolarization caused by a bAP was sufficient for all spines to relieve the Mg^{2+} block of NMDARs. Although the Ca^{2+} influx through VDCCs decreased with the distance from the soma, the influx through NMDARs counteracted this effect, resulting in a stereotyped, almost constant, spine Ca^{2+} signal during coincident EPSPs and APs.

Supralinear Ca^{2+} signals are restricted to the spine head

The large Ca^{2+} influx evoked by pairing an EPSP with a bAP was restricted to the spine head. Figure 7*A* shows a $[Ca^{2+}]$ transient measured in a spine and shaft (shown in Fig. 1) that was evoked by the sequence AP–EPSP, with an interval of 20 msec ($\Delta t = -20$ msec). The peak amplitude in the shaft corresponded well with the bAP-evoked $[Ca^{2+}]$ transient, and it was substantially smaller than the $[Ca^{2+}]$ transient in the spine head. The reverse sequence EPSP–AP at the same interval ($\Delta t = 20$ msec) evoked an even larger, supralinear Ca^{2+} signal, which was also restricted to the spine head. On average, the peak $[Ca^{2+}]$ transient in the shaft during coincident EPSP and bAP was 32 ± 10% of the $[Ca^{2+}]$ transient in the spine head ($n = 3$) and corresponded to the bAP-evoked $[Ca^{2+}]$ transient in the shaft. The supralinear Ca^{2+} signal was highly localized and restricted to the site of the active synaptic contact, where it originated with only a small accumulation of Ca^{2+} in the adjacent shaft. Thus, spines compartmentalize Ca^{2+} also during coincident activity and briefly generate a large $[Ca^{2+}]$ gradient between the synaptic spine head and the adjacent dendritic segment.

Influence of ionotropic glutamate receptors on EPSP-evoked $[Ca^{2+}]$ transients

Spine $[Ca^{2+}]$ transients evoked by EPSPs were strongly reduced in the presence of the AMPAR antagonist NBQX (10 μM) (Fig. 8*A*). The distribution of the remaining $[Ca^{2+}]$ transients after bath application of NBQX, compared with control, varied over a wide range, between 0 and 60%. In 3 of 11 spines the $[Ca^{2+}]$ transient was blocked to <8% or even abolished (Fig. 8*B*). On average, NBQX reduced the Ca^{2+} signal to 27 ± 18% ($n = 11$; $p < 0.0001$) and the EPSP to 34 ± 28% ($p < 0.00005$) of control (at −71 ± 3 mV) (Fig. 8*C*). The additional application of APV (25 μM) abolished the remaining $[Ca^{2+}]$ transient completely and reduced the EPSP amplitude to 7 ± 1% of control ($n = 3$). The remaining EPSP (0.6 ± 0.2 mV) was presumably evoked by inhibitory inputs, which were depolarizing at a resting membrane potential of −71 mV and an internal $[Cl^-]$ of 20 mM.

APV (25 μM) applied without NBQX blocked the Ca^{2+} signal to 4 ± 3% of control ($n = 4$; paired *t* test; $p < 0.02$), whereas the

EPSP amplitude was reduced much less, to 66 ± 17% of control ($p < 0.02$).

Pharmacological dissection of supralinear Ca^{2+} influx

To dissect the mechanism causing supralinearity, the $[Ca^{2+}]$ transients during coincident presynaptic and postsynaptic APs were measured in the presence of specific antagonists of glutamate receptor subtypes.

Figure 9*A* illustrates the effect of NBQX and APV on supralinear spine $[Ca^{2+}]$ transients. In this experiment, the Ca^{2+} influx during synaptic stimulation was blocked by NBQX (same experiment as that illustrated in Fig. 8*A*). When synaptic stimulation was paired with a single bAP at an interstimulus time interval of 10 msec, a large $[Ca^{2+}]$ transient was recorded again (middle trace; $A_{paired,\ NBQX} = 1.1$). Its size was similar to the transient measured under control conditions ($A_{paired,\ control} = 0.9$). Subsequent application of APV reduced the Ca^{2+} influx to a level that was similar to the bAP-evoked $[Ca^{2+}]$ transient (right trace).

NBQX had no influence on the peak $[Ca^{2+}]$ transient evoked by pairing EPSP and AP at $\Delta t = 10$ msec (reduction, compared with control, 90 ± 23%; $p > 0.1$; $n = 5$) (Fig. 9*B*). The peak $[Ca^{2+}]$ transient for the sequence AP–EPSP at $\Delta t = -10$ msec corresponded to the linear sum of the AP-evoked and the reduced EPSP-evoked $[Ca^{2+}]$ transients (nonlinearity factor = 0.9 ± 0.2; $p > 0.2$; $n = 5$).

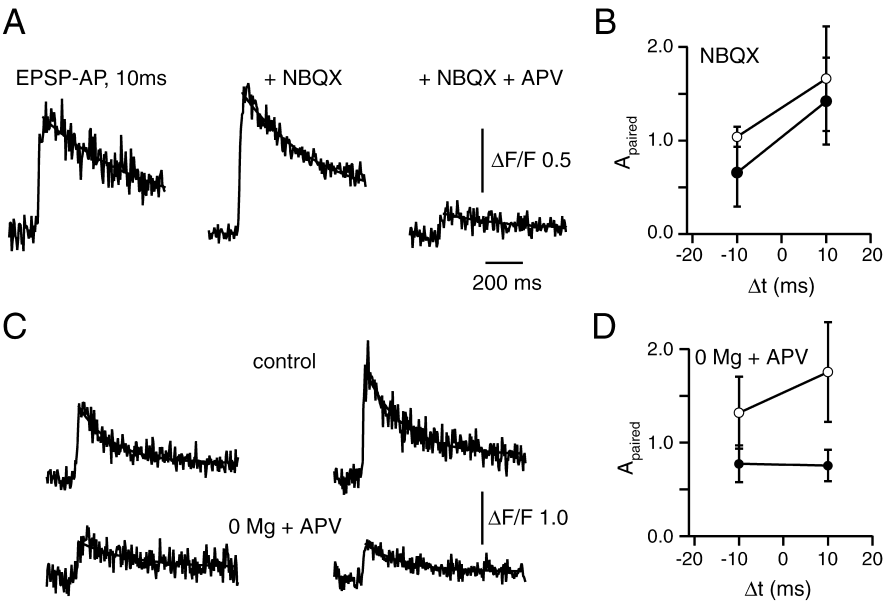

Figure 9. Influence of glutamate-receptor channels on synaptic $[Ca^{2+}]$ transients during coincident activity. *A*, Pairing an EPSP with an AP at a time interval of 10 msec in the same experiment as that depicted in Figure 8*A* resulted in a supralinear $[Ca^{2+}]$ transient (left trace). After the application of NBQX and the complete block of the EPSP-evoked $[Ca^{2+}]$ transient, this stimulation pattern resulted in the full restoration of the $[Ca^{2+}]$ transient compared with control (middle trace). The addition of APV blocked the supralinear $[Ca^{2+}]$ transient down to AP control levels (right trace). *B*, Average peak $[Ca^{2+}]$ transient amplitude, A_{paired}, measured for pairing an EPSP with an AP at time intervals of ±10 msec for control conditions (open circles) and after bath application of NBQX (filled circles). There was no significant difference between A_{paired} for control and after blocking AMPARs at $\Delta t = 10$ msec. *C*, The sequence sensitivity for pairing an EPSP with an AP at $\Delta t = \pm 10$ msec was abolished by relieving the Mg^{2+} block of the NMDAR. The top traces show the control $[Ca^{2+}]$ transients for the sequences AP–EPSP (left) and EPSP–AP (right). The peak amplitudes were 1.4 and 2.0, respectively. The sequences became indistinguishable ($A_{paired} = 0.7$ in both cases) after the washout of Mg^{2+} together with bath application of a subsaturating concentration of APV (5 μM; lower traces). *D*, Average peak $[Ca^{2+}]$ transient amplitudes for pairing an EPSP with an AP at time intervals ±10 msec for control conditions (open circles) and after washout of Mg^{2+} and bath application of a subsaturating concentration of APV (filled circles).

Figures 8*A* and 9*A* thus demonstrate that in a spine with a small or no AMPAR-dependent EPSP, which did not respond with a $[Ca^{2+}]$ transient during synaptic stimulation, a full-sized Ca^{2+} influx was evoked when synaptic stimulation was near-coincident with a bAP. This behavior is reminiscent of "silent synaptic contacts" (Liao et al., 1995).

APV reduced the Ca^{2+} influx evoked by any pairing sequence (-20 msec $< \Delta t < 20$ msec) to the size of the corresponding bAP-evoked $[Ca^{2+}]$ transient ($n = 7$). Thus, by blocking NMDAR channels, the effect of the order of pairing EPSP and AP on Ca^{2+} influx became insignificant.

Next, we tested the hypothesis that the bAP relieved the Mg^{2+} block of NMDARs, resulting in supralinear Ca^{2+} influx. $[Ca^{2+}]$ transients evoked by pairing an EPSP with a bAP at $\Delta t = \pm 10$ msec were measured in 1 mM Mg^{2+} and in Mg^{2+}-free solution. The EPSP-evoked $[Ca^{2+}]$ transient increased fourfold after the washout of Mg^{2+} ($n = 2$). To avoid saturation of the indicator dye, a subsaturating concentration of APV (5 μM) was added to the bath, resulting in a reduction of the EPSP-evoked $[Ca^{2+}]$ transient to 70% of control in 1 mM Mg^{2+} ($n = 4$). The peak $[Ca^{2+}]$ transient amplitudes for the sequences AP–EPSP and EPSP–AP at $\Delta t = \pm 10$ msec became indistinguishable in 0 Mg^{2+} ($A_{paired} = 0.7 \pm 0.2$ in both cases) (Fig. 9*C*,*D*) and corresponded to the expected linear sum. The nonlinearity factor for both sequences was 1.0 ± 0.2. Thus, the relief of NMDAR channels from the Mg^{2+} block abolished the supralinear summation of Ca^{2+} signals.

Influence of metabotropic glutamate receptors on $[Ca^{2+}]$ transients

Spiny neurons express group II metabotropic glutamate receptors (mGluRs), which contribute to the induction of changes in synaptic efficacy (Egger et al., 1999). The effect of the mGluR II antagonist EGlu (50 μM) on the $[Ca^{2+}]$ transients in spines during synaptic stimulation and coincident activity was tested to find out whether mGluRs shape spine $[Ca^{2+}]$ transients.

The $[Ca^{2+}]$ transient evoked by synaptic stimulation was not significantly reduced (82 ± 14% of control; $p > 0.2$; $n = 4$) after bath application of EGlu. The somatically recorded EPSP amplitude was also not reduced (92 ± 18% of control; $p > 0.4$) (Fig. 8*C*). $[Ca^{2+}]$ transients evoked by pairing an EPSP with a bAP at $\Delta t = \pm 20$ msec were also not affected by EGlu (Fig. 10*A*,*B*). The $[Ca^{2+}]$ transient for the sequence AP–EPSP was 89 ± 19% compared with control (paired *t* test; $p > 0.05$; $n = 3$). The $[Ca^{2+}]$ transient for the sequence EPSP–AP was 87 ± 12% compared with control ($p > 0.05$; $n = 3$). These results exclude a direct effect of mGluRs on generating $[Ca^{2+}]$ transients within a time window of ±20 msec.

In conclusion, blocking different GluR subtypes indicated that only the NMDAR contributes to the supralinear summation of synaptic Ca^{2+} signals evoked by EPSPs and bAPs during coincident presynaptic and postsynaptic APs.

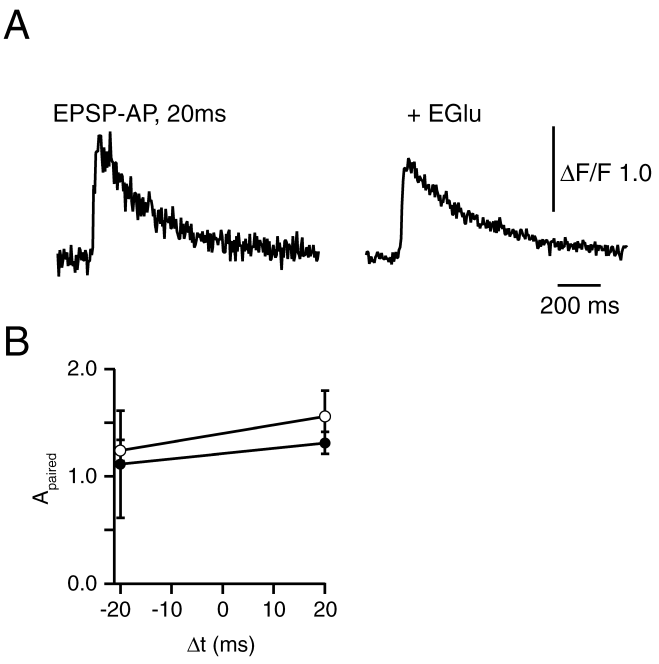

Figure 10. Influence of mGluRs on $[Ca^{2+}]$ transients during coincident activity. *A*, $[Ca^{2+}]$ transients evoked by the sequence EPSP–AP at $\Delta t = 20$ msec for control (left trace) and after bath application of EGlu (right trace). The peak amplitudes were $A_{paired} = 1.4$ for control and $A_{paired} = 1.2$ with EGlu, respectively. *B*, Average peak $[Ca^{2+}]$ transient amplitudes for pairing an EPSP with an AP at a time interval ± 20 msec for control conditions (open circles) and after bath application of EGlu. EGlu had, on average, no effect on the peak $[Ca^{2+}]$ transient amplitude.

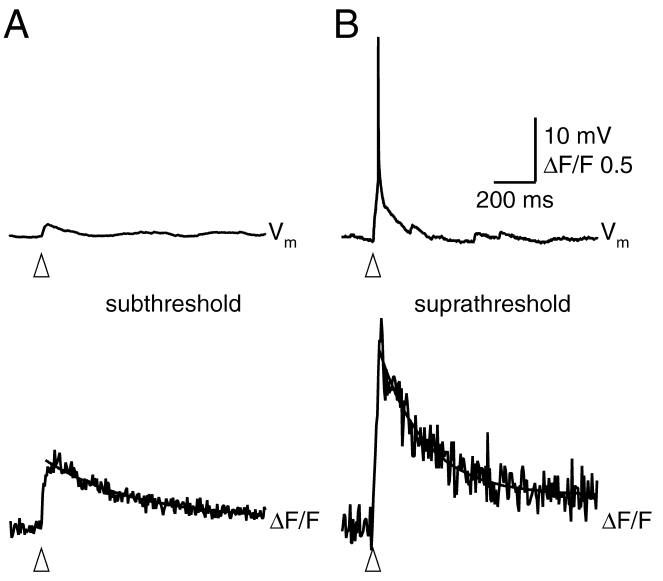

Figure 11. Suprathreshold $[Ca^{2+}]$ transients. *A*, Somatic voltage recording of a subthreshold EPSP (top trace) and the corresponding $[Ca^{2+}]$ transient. The resting membrane potential was −67 mV. The arrowhead depicts the time of stimulus onset. *B*, Increasing the stimulation strength resulted in an initial large EPSP followed by a spike ~20 msec after the onset of stimulation, reminiscent of *in vivo* recordings of spiny neurons after whisker stimulation. The corresponding $[Ca^{2+}]$ transient is similar to a $[Ca^{2+}]$ transient evoked by the stimulation sequence EPSP–AP at a interstimulus interval of 20 msec.

Suprathreshold stimulation

Finally a supralinear Ca^{2+} signal was also observed when stimulation of the synaptic input elicited an AP, a condition reminiscent of the *in vivo* situation (Fig. 11) ($n = 3$). The large EPSP (10–15 mV) evoked an AP ~15–25 msec after the EPSP onset as it is observed in adult spiny stellate neurons *in vivo* after whisker stimulation (Brecht and Sakmann, 2002b). The spine $[Ca^{2+}]$ transient evoked by suprathreshold synaptic stimulation in the acute slice preparation was much larger ($A_{suprathreshold} = 1.6$; $\tau = 225$ msec) than the $[Ca^{2+}]$ transient after subthreshold stimulation ($A_{EPSP} = 0.5$; $\tau_{EPSP} = 437$ msec) measured in the same spine.

Discussion

Backpropagating action potentials

Spiny cells in L4 of the barrel cortex belong to the class of neocortical neurons in which APs, when initiated in the soma–initial-axon segment backpropagate into the dendritic arbor and evoke a transient rise in dendritic $[Ca^{2+}]$ (Stuart and Sakmann, 1994; Markram et al., 1995; Spruston et al., 1995b). Thus, the AP output of a spiny stellate neuron in L4 that projects its axon collaterals within a column predominantly within L4, to L2/3, and to L5A (Feldmeyer et al., 2002; Lübke et al., 2003) is copied also to the dendritic arbor and encodes a transient elevation of $[Ca^{2+}]$ ["calcium code" (Magee and Johnston, 1995)]. Spiny stellate cells, like pyramidal neurons (Schiller et al., 1995; Spruston et al., 1995b; Köster and Sakmann, 1998) and inhibitory neurons in cortical layer 2/3 (Kaiser et al., 2001), which have long, electrically excitable dendrites, are endowed with this mechanism of feedback signaling to active synapses when presynaptic and postsynaptic APs are near coincident.

The spatial profile of the bAP-evoked $[Ca^{2+}]$ transient along the electrotonically compact dendritic arbor of spiny stellate cells is different from the spatial profile along the longer apical dendrite and tuft of L5 and L2/3 pyramidal neurons, where single APs do not propagate fully into the tuft and only more complex AP burst patterns result in full backpropagation and large $[Ca^{2+}]$ transients (Larkum and Zhu, 2002; Waters et al., 2003). The dendrites of spiny stellate neurons are, in this aspect, comparable to the basal dendrites of L2/3 pyramidal cells (Köster and Sakmann, 2000).

Spine-restricted $[Ca^{2+}]$ transients

In contrast to the global Ca^{2+} signal evoked by a bAP, the EPSP-evoked $[Ca^{2+}]$ transient was input-specific and restricted to an active spine head, similar to CA1 pyramidal neurons (Yuste and Denk, 1995) and L5 pyramids (Köster and Sakmann, 1998). This indicates that the Ca^{2+} accumulation in the spine head is much larger than in the adjacent shaft during synaptic activity and might be explained by negligible diffusion of Ca^{2+} across the spine neck (Svoboda et al., 1996; Yuste et al., 1999; Sabatini et al., 2002). Alternatively, the dendritic shaft might act as a large Ca^{2+} sink, which cannot accumulate Ca^{2+}. The EPSP-evoked Ca^{2+} influx into a spine was mediated mainly by NMDAR channels because the $[Ca^{2+}]$ transient was blocked during bath application of APV. The peak EPSP recorded at the soma was reduced only slightly, excluding a major contribution of VDCCs to the Ca^{2+} influx during synaptic activity (Markram and Sakmann, 1994; Schiller et al., 1998; Kovalchuk et al., 2000). The EPSP-evoked $[Ca^{2+}]$ transient in spiny stellate neurons was much more sensitive to the block of AMPARs than EPSP-evoked $[Ca^{2+}]$ transients in L5 pyramidal neurons (Köster and Sakmann, 1998) and hippocampal CA1 pyramidal neurons (Kovalchuk et al., 2000). This difference might be caused by the resting membrane potential and different NMDAR/AMPAR channel ratios (Markram et al., 1997b; Feldmeyer and Sakmann, 2000).

Coincidence detection by spines

Spines of spiny neurons can act, as in other neocortical cells (Yuste and Denk, 1995; Köster and Sakmann, 1998; Yuste et al., 1999), as detectors for near-coincident presynaptic and postsynaptic APs that evoke a large $[Ca^{2+}]$ transient because of supralinear summation within a short time window of <50 msec. The pharmacological effects of GluR-channel antagonists strongly suggest that the major mechanism generating the large Ca^{2+} influx is unblocking of NMDAR channels by dendritic depolarization. This view is supported by the observation that removing Mg^{2+} from the bath abolished the supralinear summation of the Ca^{2+} signals and that the supralinearity decayed with a time constant comparable to the deactivation kinetics of the NMDAR channel in juvenile (P14) spiny stellate neurons.

Because the nonlinearity factor and the peak $[Ca^{2+}]$ transient amplitude for the sequence EPSP–AP at intervals of 10 msec is independent of the distance between the spine and the soma, the Ca^{2+} signals evoked during coincident activity represent a common and almost uniform signal for all active spines along the dendritic arbor. The large spinous Ca^{2+} accumulation during coincident activity is restricted to the active site representing a locally confined and input-specific signal.

The sublinear summation of the Ca^{2+} signals for the sequence AP–EPSP at intervals of −50 msec could reflect Ca^{2+}-dependent inactivation of NMDAR channels (Legendre et al., 1993; Umemiya et al., 2001).

Because the postsynaptic $[Ca^{2+}]$ transients in spines were evoked by extracellular stimulation in L4, we do not know which presynaptic afferents were stimulated. It was estimated that 10–20% of the excitatory synaptic contacts onto spiny stellate cells are thalamocortical (Benshalom and White, 1986). Most of the rest are corticocortical connections, originating mainly from other spiny stellate cells (Feldmeyer et al., 1999). In either case the results for supralinear Ca^{2+} influx are likely to be the same because the properties of the NMDAR of spiny stellate cells are independent of the projecting afferents (Gil et al., 1999).

Connections between spiny stellate cells express long-term depression (LTD) independent of spike-timing (Egger et al., 1999), whereas the same pairing protocols resulted in induction of long-term potentiation and LTD depending on the order of stimuli in L5 pyramidal neurons (Markram et al., 1997a). We find that Ca^{2+}-signaling in spines of L4 spiny stellates is similar to that in L5 pyramidal neurons (Köster and Sakmann, 1998). In both cell types, coincident activity results in a large rise in $[Ca^{2+}]$, which suggests that different cell types might decode increased $[Ca^{2+}]$ levels differently via NMDAR-independent pathways, such as mGluRs (Anwyl, 1999; Karmarkar and Buonomano, 2002).

Silent synaptic contacts

Putative electrically "silent synapses" are postulated to exist in connections of the developing postnatal (P6–P7) somatosensory (Isaac et al., 1995), and visual (Rumpel et al., 1998) cortex. Here, a fraction of the synaptic contacts are thought to possess mostly NMDARs but no functional AMPARs in their spine heads. At resting membrane potential, these synaptic contacts do not contribute (or contribute only very little) to EPSPs. Blocking the AMPARs in spiny stellate cells pharmacologically created a comparable experimental condition. The Ca^{2+} influx into individual spines evoked by subthreshold synaptic stimulation was strongly reduced, resulting in "Ca^{2+}-silent" spines. Surprisingly, a large Ca^{2+} influx reappeared when synaptic stimulation was coincident with a bAP within a time interval of <20 msec. We conclude that electrically silent spines without functional AMPARs can nevertheless transmit synaptic signals by generating large $[Ca^{2+}]$ transients when coincident activation of other synapses evokes bAPs. This bAP-dependent spine Ca^{2+} signal could render silent synapses functional at least with respect to Ca^{2+}-dependent dendritic mechanisms (Liao et al., 1995; Isaac et al., 1997; Malinow et al., 2000; Poncer and Malinow, 2001).

Physiological relevance of bAPs and spine Ca^{2+} transients for spiny cells in L4

Spiking of excitatory neurons in L4 of the barrel cortex is sparse, and whisker stimulation elicits only few APs in L4 neurons (Bruno and Simons, 2002). However, *in vivo* wc recordings from stellate cells in the barrel cortex indicate that a compound EPSP with >10 mV depolarization, when evoked by a whisker deflection, can trigger an AP within a few tens of msec (Brecht and Sakmann, 2002b). Thus, *in vivo* in those spines, which contribute to AP initiation, the EPSP–AP sequence will cause a large transient increase in $[Ca^{2+}]$. Whether the coincidence of a compound EPSP and the bAP, when evoked by sensory stimulation, attenuates or enhances the efficacy of the thalamocortical (VPM-to-L4) or the corticocortical (L4-to-L4) connections is as yet unclear. Studies with CxNR1 knock-out mice indicate that NMDARs are essential for normal development and the anatomical patterning of the barrel cortex (Datwani et al., 2002).

Thalamocortical afferents from a single neuron in VPM can project to the principle whisker (PW) barrel and surround whisker (SuW) barrels (Arnold et al., 2001). The EPSPs evoked in L4 cells by PW or SuW deflection are delayed with respect to each other (Brecht and Sakmann, 2002b). Furthermore, SuW stimulation only infrequently evokes an AP in L4 cells. Thus, if large coincidence-dependent dendritic $[Ca^{2+}]$ transients were controlling synaptic strength in L4 spiny stellates, only those synaptic contacts that, when activated, contribute to the initiation of an AP would also be modified. Such a coincidence-based mechanism for altering synaptic efficacy could operate both during the development of barrel columns in the early postnatal time as well as in the adult cortex.

References

Agmon A, Connors BW (1991) Thalamocortical responses of mouse somatosensory (barrel) cortex in vitro. Neuroscience 41:365–379.

Anwyl R (1999) Metabotropic glutamate receptors: electrophysiological properties and role in plasticity. Brain Res Brain Res Rev 29:83–120.

Arnold PB, Li CX, Waters RS (2001) Thalamocortical arbors extend beyond single cortical barrels: an in vivo intracellular tracing study in rat. Exp Brain Res 136:152–168.

Bekkers JM, Stevens CF (1989) NMDA and non-NMDA receptors are colocalized at individual excitatory synapses in cultured rat hippocampus. Nature 341:230–233.

Benshalom G, White EL (1986) Quantification of thalamocortical synapses with spiny stellate neurons in layer IV of mouse somatosensory cortex. J Comp Neurol 253:303–314.

Brecht M, Sakmann B (2002a) Whisker maps of neuronal subclasses of the rat ventral posterior medial thalamus, identified by whole-cell voltage recording and morphological reconstruction. J Physiol (Lond) 538:495–515.

Brecht M, Sakmann B (2002b) Dynamic representation of whisker deflection by synaptic potentials in spiny stellate and pyramidal cells in the barrels and septa of layer 4 rat somatosensory cortex. J Physiol (Lond) 543:49–70.

Bruno RM, Simons DJ (2002) Feedforward mechanisms of excitatory and inhibitory cortical receptive fields. J Neurosci 22:10966–10975.

Datwani A, Iwasato T, Itohara S, Erzurumlu RS (2002) NMDA receptor-dependent pattern transfer from afferents to postsynaptic cells and dendritic differentiation in the barrel cortex. Mol Cell Neurosci 21:477–492.

Denk W, Strickler JH, Webb WW (1990) Two-photon laser scanning fluorescence microscopy. Science 248:73–76.

Denk W, Yuste R, Svoboda K, Tank DW (1996) Imaging calcium dynamics in dendritic spines. Curr Opin Neurobiol 6:372–378.

Dodt H, Eder M, Frick A, Zieglgänsberger W (1999) Precisely localized LTD in the neocortex revealed by infrared-guided laser stimulation. Science 286:110–113.

Dodt HU, Zieglgänsberger W (1998) Visualization of neuronal form and function in brain slices by infrared videomicroscopy. Histochem J 30:141–152.

Egger V, Feldmeyer D, Sakmann B (1999) Coincidence detection and changes of synaptic efficacy in spiny stellate neurons in rat barrel cortex. Nat Neurosci 2:1098–1105.

Feldman DE (2000) Timing-based LTP and LTD at vertical inputs to layer II/III pyramidal cells in rat barrel cortex. Neuron 27:45–56.

Feldmeyer D, Sakmann B (2000) Synaptic efficacy and reliability of excitatory connections between the principal neurones of the input (layer 4) and output layer (layer 5) of the neocortex. J Physiol (Lond) 525:31–39.

Feldmeyer D, Egger V, Lübke J, Sakmann B (1999) Reliable synaptic connections between pairs of excitatory layer 4 neurones within a single "barrel" of developing rat somatosensory cortex. J Physiol (Lond) 521:169–190.

Feldmeyer D, Lübke J, Silver RA, Sakmann B (2002) Synaptic connections between layer 4 spiny neurone-layer 2/3 pyramidal cell pairs in juvenile rat barrel cortex: physiology and anatomy of interlaminar signalling within a cortical column. J Physiol (Lond) 538:803–822.

Gil Z, Connors BW, Amitai Y (1999) Efficacy of thalamocortical and intracortical synaptic connections: quanta, innervation, and reliability. Neuron 23:385–397.

Helmchen F, Imoto K, Sakmann B (1996) Ca^{2+} buffering and action potential-evoked Ca^{2+} signaling in dendrites of pyramidal neurons. Biophys J 70:1069–1081.

Isaac JT, Nicoll RA, Malenka RC (1995) Evidence for silent synapses: implications for the expression of LTP. Neuron 15:427–434.

Isaac JT, Crair MC, Nicoll RA, Malenka RC (1997) Silent synapses during development of thalamocortical inputs. Neuron 18:269–280.

Johnson JW, Ascher P (1987) Glycine potentiates the NMDA response in cultured mouse brain neurons. Nature 325:529–531.

Kaiser KM, Zilberter Y, Sakmann B (2001) Back-propagating action potentials mediate calcium signalling in dendrites of bitufted interneurons in layer 2/3 of rat somatosensory cortex. J Physiol (Lond) 535:17–31.

Karmarkar UR, Buonomano DV (2002) A model of spike-timing dependent plasticity: one or two coincidence detectors? J Neurophysiol 88:507–513.

Köster HJ, Sakmann B (1998) Calcium dynamics in single spines during coincident presynaptic and postsynaptic activity depend on relative timing of back-propagating action potentials and subthreshold excitatory postsynaptic potentials. Proc Natl Acad Sci USA 95:9596–9601.

Köster HJ, Sakmann B (2000) Calcium dynamics associated with action potentials in single nerve terminals of pyramidal cells in layer 2/3 of the young rat neocortex. J Physiol (Lond) 529 Pt 3:625–646.

Köster HJ, Baur D, Uhl R, Hell SW (1999) Ca^{2+} fluorescence imaging with pico- and femtosecond two-photon excitation: signal and photodamage. Biophys J 77:2226–2236.

Kovalchuk Y, Eilers J, Lisman J, Konnerth A (2000) NMDA receptor-mediated subthreshold Ca^{2+} signals in spines of hippocampal neurons. J Neurosci 20:1791–1799.

Larkum ME, Zhu JJ (2002) Signaling of layer 1 and whisker-evoked Ca^{2+} and Na^{+} action potentials in distal and terminal dendrites of rat neocortical pyramidal neurons *in vitro* and *in vivo*. J Neurosci 22:6991–7005.

Legendre P, Rosenmund C, Westbrook GL (1993) Inactivation of NMDA channels in cultured hippocampal neurons by intracellular calcium. J Neurosci 13:674–684.

Liao D, Hessler NA, Malinow R (1995) Activation of postsynaptically silent synapses during pairing-induced LTP in CA1 region of hippocampal slice. Nature 375:400–404.

Lübke J, Egger V, Sakmann B, Feldmeyer D (2000) Columnar organization of dendrites and axons of single and synaptically coupled excitatory spiny neurons in layer 4 of the rat barrel cortex. J Neurosci 20:5300–5311.

Lübke J, Roth A, Feldmeyer D, Sakmann B (2003) Morphometric analysis of the columnar innervation domain of neurons connecting layer 4 and layer 2/3 of juvenile rat barrel cortex. Cereb Cortex 13:1051–1063.

Magee JC, Johnston D (1995) Characterization of single voltage-gated Na^{+} and Ca^{2+} channels in apical dendrites of rat CA1 pyramidal neurons. J Physiol (Lond) 487:67–90.

Malinow R, Mainen ZF, Hayashi Y (2000) LTP mechanisms: from silence to four-lane traffic. Curr Opin Neurobiol 10:352–357.

Markram H, Sakmann B (1994) Calcium transients in dendrites of neocortical neurons evoked by single subthreshold excitatory postsynaptic potentials via low-voltage-activated calcium channels. Proc Natl Acad Sci USA 91:5207–5211.

Markram H, Helm PJ, Sakmann B (1995) Dendritic calcium transients evoked by single back-propagating action potentials in rat neocortical pyramidal neurons. J Physiol (Lond) 485:1–20.

Markram H, Lübke J, Frotscher M, Sakmann B (1997a) Regulation of synaptic efficacy by coincidence of postsynaptic APs and EPSPs. Science 275:213–215.

Markram H, Lübke J, Frotscher M, Roth A, Sakmann B (1997b) Physiology and anatomy of synaptic connections between thick tufted pyramidal neurones in the developing rat neocortex. J Physiol (Lond) 500:409–440.

Petersen CC, Sakmann B (2000) The excitatory neuronal network of rat layer 4 barrel cortex. J Neurosci 20:7579–7586.

Petersen CC, Sakmann B (2001) Functionally independent columns of rat somatosensory barrel cortex revealed with voltage-sensitive dye imaging. J Neurosci 21:8435–8446.

Poncer JC, Malinow R (2001) Postsynaptic conversion of silent synapses during LTP affects synaptic gain and transmission dynamics. Nat Neurosci 4:989–996.

Rathenberg J, Nevian T, Witzemann V (2003) High-efficiency transfection of individual neurons using modified electrophysiology techniques. J Neurosci Methods 126:91–98.

Rumpel S, Hatt H, Gottmann K (1998) Silent synapses in the developing rat visual cortex: evidence for postsynaptic expression of synaptic plasticity. J Neurosci 18:8863–8874.

Sabatini BL, Oertner TG, Svoboda K (2002) The life cycle of Ca^{2+} ions in dendritic spines. Neuron 33:439–452.

Schiller J, Helmchen F, Sakmann B (1995) Spatial profile of dendritic calcium transients evoked by action potentials in rat neocortical pyramidal neurones. J Physiol (Lond) 487:583–600.

Schiller J, Schiller Y, Clapham DE (1998) NMDA receptors amplify calcium influx into dendritic spines during associative presynaptic and postsynaptic activation. Nat Neurosci 1:114–118.

Silver RA, Lübke J, Sakmann B, Feldmeyer D (2003) High probability uniquantal transmission at excitatory synapses in barrel cortex. Science, in press.

Spruston N, Jonas P, Sakmann B (1995a) Dendritic glutamate receptor channels in rat hippocampal CA3 and CA1 pyramidal neurons. J Physiol (Lond) 482:325–352.

Spruston N, Schiller Y, Stuart G, Sakmann B (1995b) Activity-dependent action potential invasion and calcium influx into hippocampal CA1 dendrites. Science 268:297–300.

Stuart GJ, Sakmann B (1994) Active propagation of somatic action potentials into neocortical pyramidal cell dendrites. Nature 367:69–72.

Stuart GJ, Dodt HU, Sakmann B (1993) Patch-clamp recordings from the soma and dendrites of neurons in brain slices using infrared video microscopy. Pflügers Arch 423:511–518.

Svoboda K, Tank DW, Denk W (1996) Direct measurement of coupling between dendritic spines and shafts. Science 272:716–719.

Umemiya M, Chen N, Raymond LA, Murphy TH (2001) A calcium-dependent feedback mechanism participates in shaping single NMDA miniature EPSCs. J Neurosci 21:1–9.

Waters J, Larkum M, Sakmann B, Helmchen F (2003) Supralinear Ca^{2+} influx into dendritic tufts of layer 2/3 neocortical pyramidal neurons *in vitro* and *in vivo*. J Neurosci 23:8558–8567.

Westenbroek RE, Ahlijanian MK, Catterall WA (1990) Clustering of L-type Ca^{2+} channels at the base of major dendrites in hippocampal pyramidal neurons. Nature 347:281–284.

Yuste R, Denk W (1995) Dendritic spines as basic functional units of neuronal integration. Nature 375:682–684.

Yuste R, Majewska A, Cash SS, Denk W (1999) Mechanisms of calcium influx into hippocampal spines: heterogeneity among spines, coincidence detection by NMDA receptors, and optical quantal analysis. J Neurosci 19:1976–1987.